DNS and RANS for core-annular flow with a turbulent annulus

Li, Haoyu; Pourquié, M. J.B.M.; Ooms, G.; Henkes, R. A.W.M.

DOI
10.1016/j.ijmultiphaseflow.2024.104733

Publication date
2024

Document Version
Final published version

Published in
International Journal of Multiphase Flow

International Journal of Multiphase Flow 174 (2024) 104733

Contents lists available at ScienceDirect

International Journal of Multiphase Flow

journal homepage: www.elsevier.com/locate/ijmulflow

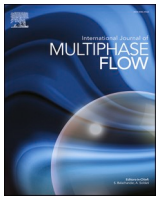

DNS and RANS for core-annular flow with a turbulent annulus

Haoyu Li, M.J.B.M. Pourquié, G. Ooms, R.A.W.M. Henkes *

Delft University of Technology, the Netherlands

ARTICLE INFO

Keywords:
Core-annular flow
Turbulent annulus flow
Two-phase DNS
Wavy interface

ABSTRACT

DNS and RANS simulations were carried out for core-annular flow in a horizontal pipe and results were compared with experiments carried out with water and oil in our lab. In contrast to most existing studies for core-annular flow available in the literature, the flow annulus is not laminar but turbulent. This makes the simulations more challenging. As DNS does not contain any closure correlations, this approach should give the best representation of the flow (provided a sufficiently accurate numerical mesh and numerical method is used). Various flow configurations were considered, such as without gravity (to enforce an on-average concentric oil core) and with gravity (to allow for eccentricity in the oil core location). Both single-phase and two-phase conditions were considered; single-phase flow refers to the water annulus with imposed wavy wall, whereas two-phase flow includes the determination of the wavy interface. Mesh refinement was carried out to assess the numerical accuracy of the simulation results.

1. Introduction

Core-annular flow (CAF) is a typical two-phase liquid-liquid flow pattern in a pipeline system. In this flow pattern, a viscous liquid core (such as oil) is surrounded by a less viscous annulus (such as water). The thin water annulus can lubricate the pipe wall, which significantly decreases the pressure drop compared to viscous oil transport. Therefore, this kind of flow pattern is applicable in transporting highly viscous oil in the petroleum industry. Furthermore, core-annular flow is also of great interest from a fundamental fluid mechanics perspective.

Over the past decades, much research was devoted to core-annular flow. Research topics included: stability of CAF, interfacial waves, prediction of pressure drop and hold up ratio, and the levitation mechanism in horizontal pipe flow. Joseph et al. (1997) and Ghosh et al. (2009) have provided reviews. In addition to lab experiments, CFD simulations can provide a detailed description of the flow phenomena. The complexity of the multiphase flow, with its liquid-liquid interface and possibly turbulent water annulus, make the numerical simulations challenging. As the oil has a much higher viscosity than water, there is a jump in the viscosity and in the velocity gradient across the interface, and the interface may dampen the turbulence in the water annulus. Besides, the apparent slip between the oil and water can cause flow instability, in which waves will develop at the interface; such waves will interact with the turbulent flow field. The precise origin of the interface instability and wave growth can be studied with a stability analysis, as was done by Li and Renardy (1999) for a laminar water annulus and by Li et al. (2023b) for a turbulent water annulus.

Li and Renardy (1999) used the Volume of Fluid (VOF) method to perform a direct numerical simulation of the laminar-laminar 2D core-annular flow, in which the instability problem and wave shape were studied. A similar numerical method was used by Ooms et al. (2013) to simulate 3D laminar-laminar. Kang et al. (2007) used the level set method for 2D axisymmetric vertical core-annular flow; they managed to simulate the "bamboo wave" with a sharp wave crest. The breaking and merging of the oil core was also simulated. Beerens et al. (2014) used the VOF method to simulate 2D laminar vertical core-annular flow. The linear wave growth was studied for shorter pipe section lengths, and multiple wave lengths were shown to appear in their long pipe simulation results. For the CAF simulation with a turbulent water annulus, Huang et al. (1994) used the low Reynolds number $k-\varepsilon$ model to simulate the velocity profile of eccentric core-annular flow. Ko et al. (2002) simulated the turbulent water annulus assuming the oil core to be solid; the solid "interface" was simulated with a similar method as applied by Bai et al. (1996). They found the SST $k-\omega$ model to perform better than the standard $k-\omega$ model. The wave length, pressure drop and secondary flow for different Reynolds numbers were simulated. Ingen Housz et al. (2017) preformed 3D simulations for horizontal CAF, using the VOF method for the interface capturing and the low Reynolds Launder–Sharma $k-\varepsilon$ model for turbulence. It is found that the water is laminar in the top layer and

* Corresponding author.
E-mail address: r.a.w.m.henkes@tudelft.nl (R.A.W.M. Henkes).

https://doi.org/10.1016/j.ijmultiphaseflow.2024.104733
Received 25 August 2023; Received in revised form 1 December 2023; Accepted 13 January 2024
Available online 29 January 2024

turbulent in the bottom water layer. When comparing the simulation results with experiments, the pressure drop and the top wave amplitude in the simulation were both lower than in the experiments. Shi et al. (2017) simulated horizontal oil-water flow in which both liquids had the same density. The VOF method is used and various flow patterns were simulated. The SST $k-\omega$ model was found to give the best results. Ghosh et al. (2010) simulated downward CAF using VOF with the $k-\varepsilon$ method, but a rather coarse mesh was used. Kim and Choi (2018) performed high-resolution DNS using the level set method for vertical core annular flow with a turbulent water annulus, and detailed flow statistics were provided. We have recently also used the RANS approach (Reynolds-Averaged Navier Stokes) for core-annular flow in different configurations (see Li et al., 2021, 2022, 2023a,b). We have paid much attention to verifying that the RANS results are numerically accurate (through successive mesh refinement). From the literature review, it becomes clear that DNS for horizontal CAF with a turbulent annulus are lacking.

Very accurate results from DNS are available for single phase pipe flow, such as Eggels et al. (1994), Wu and Moin (2008), and Pirozzoli et al. (2021). These studies provide a good reference to validate the performance of our current DNS. The interaction of the turbulent water annulus with the oil-water interface is an interesting phenomenon in core-annular flow, which has not been simulated very often so far. Sullivan et al. (2000) and Buckley et al. (2016) studied the interaction of turbulent air flow with an idealized water wave; here the wave-correlated velocity, and the critical layer of the turbulent momentum flux are studied for different wave speeds. The three contributions to the total stress (i.e. the turbulent stress, wave-induced stress, and viscous stress) are discussed separately by Yousefi et al. (2020). They found a wave-induced transfer of energy between the waves and the turbulent annulus flow and between the mean flow and the wave motion. The interaction of waves and turbulence in the oil-water scenario can be different compared to that in air-water, due to the lack and presence of the effect of gravity, respectively. Recently, Giamagas et al. (2023) carried out a detailed numerical study for the waves and turbulence at the interface of stratified oil-water flow in a channel.

The main purpose of the present paper is to perform DNS for horizontal oil-water core-annular flow, and compare the results with RANS results. From the DNS, detailed flow characteristics can be shown. The comparison between DNS and RANS is first performed for single-phase pipe flow. Then, the single-phase annulus flow is simulated to show the effect of waves on the turbulent annulus flow. Finally, DNS are performed for the two-phase CAF both with and without gravity. The DNS results are compared with the RANS simulation results and with lab experiments.

2. Method

2.1. Governing equations

The mass and momentum conservation equations for an incompressible, isothermal fluid are (in Cartesian coordinates):

$$\frac{\partial u_i}{\partial x_i}=0 \tag{1}$$

$$\frac{\partial \rho u_i}{\partial t}+\rho u_j\frac{\partial u_i}{\partial x_j}=\frac{\partial}{\partial x_j}\left(\rho(\nu+\nu_t)\left(\frac{\partial u_i}{\partial x_j}+\frac{\partial u_j}{\partial x_i}\right)\right)-\frac{\partial p}{\partial x_i}+\rho g_i+F_{\sigma,i} \tag{2}$$

Here u_i is the velocity, ρ and μ are the fluid density and viscosity, g_i is the gravitational acceleration, p is the pressure and $F_{\sigma,i}$ is the interfacial tension force. For the pipe flow, we will use $x_1=x$ for the coordinate along the horizontal pipe axis, $x_2=y$ for the vertical coordinate, and $x_3=z$ for the coordinate in the horizontal plane perpendicular to x; the velocity components are u, v, and w, in the directions x, y, and z, respectively. The gravity components are: g_1=g_3=0, and $g_2=-g$, where g is the gravitational acceleration. Both 2D and 3D simulations were carried out. All 2D simulations applied axi-symmetric coordinates with the radius $r=\sqrt{y^2+z^2}$.

For the RANS simulations, Eq. (2) is the Reynolds-Averaged Navier-Stokes Equation, in which the turbulent viscosity ν_t is modeled using the low-Reynolds number $k-\varepsilon$ model of Launder and Sharma (1974):

$$\nu_t=C_\mu f_\mu\frac{k^2}{\widetilde{\varepsilon}} \tag{3}$$

$$\frac{\partial k}{\partial t}+u_j\frac{\partial k}{\partial x_j}=\frac{\partial}{\partial x_j}\left(\nu+\frac{\nu_t}{\sigma_k}\right)\frac{\partial k}{\partial x_j}+\nu_t\left(\frac{\partial u_j}{\partial x_j}\right)^2-\widetilde{\varepsilon}-D \tag{4}$$

$$\frac{\partial \widetilde{\varepsilon}}{\partial t}+u_j\frac{\partial \widetilde{\varepsilon}}{\partial x_j}=\frac{\partial}{\partial x_j}\left(\nu+\frac{\nu_t}{\sigma_\varepsilon}\right)\frac{\partial \widetilde{\varepsilon}}{\partial x_j}+C_1f_1\frac{\widetilde{\varepsilon}}{k}\nu_t\left(\frac{\partial u_j}{\partial x_j}\right)^2-C_2f_2\frac{\widetilde{\varepsilon}^2}{k}+E \tag{5}$$

With $D=2\nu\frac{\partial\sqrt{k}}{\partial x_j}\frac{\partial\sqrt{k}}{\partial x_j}$ and $E=2\nu\nu_t\left(\frac{\partial^2 u_j}{\partial x_j^2}\right)^2$. The turbulent energy dissipation rate is $\varepsilon=\widetilde{\varepsilon}+D$. Furthermore, $C_\mu=0.09$, C_1=1.44, C_2=1.92, σ_k=1.0, σ_ε=1.3, $f_\mu=\exp\left(\frac{-3.4}{\left(1+\frac{Re_t}{50}\right)^2}\right)$, f_1=1, $f_2=1-0.3\exp(-Re_t^2)$, $Re_t=\frac{k^2}{\varepsilon\nu}$. The boundary conditions at the wall are: k=0 and $\widetilde{\varepsilon}=0$.

Within DNS, ν_t will be removed from Eq. (2), and all scales of turbulence flow are directly simulated.

2.2. Numerical method

The open-source package OpenFOAM is used for solving the governing equations, in which the CLSVOF method is used for interface capturing. The CLSVOF solver, which was developed by Yamamoto et al. (2017), is based on the interFOAM Volume of Fluid (VOF) solver in OpenFOAM. The level set function is used to calculate the interfacial tension force. Starting from the VOF method, the volume fraction α is introduced to distinguish between the two fluid phases: $\alpha=0$ is the oil phase, $\alpha=1$ is the water phase, and $0<\alpha<1$ denotes the oil-water interface. Herewith, the fluid density and viscosity in the equations are:

$$\rho=(1-\alpha)\rho_o+\alpha\rho_w \tag{6}$$

$$\mu=(1-\alpha)\mu_o+\alpha\mu_w \tag{7}$$

The subscript "o" refers to oil, and the subscript "w" refers to water. α is calculated from the following advection equation:

$$\frac{\partial\alpha}{\partial t}+\nabla\cdot(\alpha\vec{u})+\nabla\cdot\left((1-\alpha)\alpha\vec{u}_r\right)=0 \tag{8}$$

The third term on the left-hand side is the compressive term (with the divergence of the compressive flux); here $\vec{u}_r=\vec{u}_w-\vec{u}_o$. This term controls the sharpness of interface; this means minimizing the number of cells perpendicular to the interface that have a value of the volume fraction α that is not pure oil ($\alpha=0$) or pure water ($\alpha=1$), while still maintaining numerical stability.

The level set function Φ is defined as the signed distance from the interface, where the interface is the isoline with $\Phi=0$. The initial value of the level set function Φ_o is obtained from the initialized volume-of-fluid field, where the interface is defined at $\alpha=0.5$:

$$\Phi_0=(2\alpha-1)\Gamma \tag{9}$$

$$\Gamma=0.75\Delta X \tag{10}$$

Here ΔX is the minimum mesh size near the interface. Thereafter the re-initialization equation is solved to turn the initial level set function into the distance from the interface:

$$\frac{\partial\Phi}{\partial\tau}=\mathrm{sign}(\Phi_0)(1-|\nabla\Phi|) \tag{11}$$

Here $\tau=0.1\Delta X$ is the iteration time step of Φ and the sign function denotes:

$$\text{sign}(\Phi) = \begin{cases} 1 \ \Phi > 0, \ water \\ 0 \ \Phi = 0, \ interface \\ -1 \ \Phi < 0, \ oil \end{cases} \tag{12}$$

Then the interface tension force is calculated as:

$$\vec{F}_\sigma = \sigma\kappa(\Phi)\delta_\Phi \nabla(\Phi) \tag{13}$$

Here σ is the interface tension and δ_Φ is the smoothed delta function:

$$\delta_\Phi = \begin{cases} \frac{1}{2\gamma}\left(1 + \cos\left(\frac{\pi\Phi}{\gamma}\right)\right) for \ |\Phi| < \gamma \\ 0 \ elsewhere \end{cases} \tag{14}$$

The quantity γ is the interface thickness coefficient (see Yamamoto et al., 2017) and $\kappa(\Phi)$is the interface curvature:

$$\kappa(\Phi) = \nabla \cdot \vec{n}_c \tag{15}$$

$$\vec{n}_c = \frac{(\nabla\Phi)_f}{\left|(\nabla\Phi)_f\right|} \tag{16}$$

Here $\vec{n}_c$ is the surface unit normal vector. The contact angle θ between the interface and the pipe wall is defined as:

$$\cos(\theta) = \vec{n}_c \cdot \vec{n}_w \tag{17}$$

With $\vec{n}_w$ being the unit normal vector at the wall. The contact angle is set to 90° in our simulations. This means that both the level set function Φ and the volume fraction of the fluid α satisfy the zero-gradient condition at the pipe wall boundary.

A pressure drop in the flow direction is added as an extra force term to the right-hand side of Eq. (2), while we use periodic boundary conditions on the left and right side of the pipe. Therefore, the pressure that remains in the equations is periodic with respect to the left and right side of the computational pipe section. The initially assumed velocity profile will then develop over time in the transient simulation under this pressure drop until a stable state is obtained. For the DNS, the initial velocity is disturbed with given energy spectrum, the built-in utility "Boxturb" in OpenFOAM is used.

A second-order backward implicit time discretization scheme is applied, with a very small time step (small Courant number). This gives a very accurate time integration. For the advection terms in the Navier-Stokes equations we use second order central differences for DNS and limited linear for RANS. For the turbulence model equations, second order upwind is used for the advection terms. For the interface advection equation the OpenFOAM MULES scheme is used. In all the simulations, periodic boundary conditions are applied on the left and right side of the pipe, which restricts the wave lengths in the axial direction to the domain length divided by an integer value. At the pipe wall, the no-slip condition is imposed. We have used the symmetric PBiCG solver for the velocity and for the turbulent quantities, the GAMG solver for the pressure, and the PIMPLE solver for the velocity-pressure coupling.

The following mesh structure was applied for both the single-phase and two-phase pipe flow simulations. The mesh is equidistant in the main flow direction. The numerical mesh in the pipe cross section consists of four regions. The first mesh region is a pentagon located in the pipe centre, with a similar structured mesh in each of the five layers. Outside the pentagon there is a second mesh region that extends to a circular boundary at one third the pipe radius. The third region start at the circular boundary from the second region and ends at a circular boundary close to the pipe wall. Here the mesh size is varied by using a radial stretching function, that smoothly expands the mesh size going from a smaller to higher local radius. The fourth layer is the ring that starts with the outer circle of the third layer and ends at the circular pipe wall. Here the radial mesh size is equidistant, such that the first mesh point falls well in the viscous sublayer. Mesh layers 1 and 2 are not fully axi-symmetric (due to the pentagon structure). Mesh layers 3 and 4 are fully axisymmetric.

2.3. Considered base conditions

The simulation conditions for two-phase CAF were the same as in the experiments carried out in our lab. The pipe radius is R=0.0105 m (pipe diameter is D=21 mm). The length of the pipe section is set to 0.0256 m (25.6 mm), which is twice the most dominant wave length, as estimated from a linear instability analysis (albeit for laminar flow) by Beerens et al. (2014). The fluid properties are set as follows: the oil and water kinematic viscosity are $\nu_o = 7.73 \times 10^{-4}$ m^2/s and $\nu_w = 6.7 \times 10^{-7}$ m^2/s, the oil and water densities are $\rho_o = 902$ kg/m^3 and $\rho_w = 993$ kg/m^3, and the interfacial tension between oil and water is $\sigma = 0.016$ N/m (Shell Morlina S2 B 680 at 40 °C was used in the experiments). Note that the ratio between the kinematic viscosities of oil and water is 1150, and the density ratio between the oil and water is $\rho_o/\rho_w = 0.91$. The Reynolds number in wall units, i.e. $Re_\tau = d^+ = u_\tau d/\nu_w$, is about 150 (here u_τ is the wall shear velocity and d is the average thickness of the water annulus). This is above the minimum value of about 90 which is needed to sustain turbulence in single phase channel flow (where d is half the channel width); this criterion was derived by Jimenez and Moin (1991), who applied DNS to channel flow. The occurrence of turbulence in the water annulus is confirmed in our previous RANS simulations (Li et al., 2021, 2022), which show an inertial sublayer with a maximum turbulent viscosity (ν_t/ν_w) of about 20.

2.4. Key parameters

Four important parameters are: the total flow rate, the pressure drop, the water cut, and the water holdup fraction. When two parameters are set as input (e.g. the total flow rate and the water cut in the experiments), the other two will follow as output.

The water cut is defined as the ratio of the water volumetric flow rate and the total volumetric flowrate:

$$\text{WC} = Q_w/(Q_o + Q_w) \tag{18}$$

where Q denotes the volumetric flow rate. The water holdup fraction is defined as the ratio of the in-situ water volume in the pipe and the total volume of oil and water:

$$\alpha_w = \frac{V_w}{V_w + V_o} \tag{19}$$

A related parameter is the so-called holdup ratio h, which is defined as:

$$h = \frac{Q_o/Q_w}{V_o/V_w} \tag{20}$$

This can also be rewritten as $h = 1 + u_r/u_w$. Here the velocity difference $u_r = u_o - u_w$, is the apparent (average) slip velocity between the oil core (having a bulk velocity u_o) and the water annulus (having a bulk velocity u_w). Note that h =1 if there is no slip between the bulk oil and water velocities. The holdup ratio thus is a measure of the apparent slip between the oil core and the water annulus.

The (total) mixture velocity is defined as:

$$U_{mix} = \frac{Q_w + Q_o}{A_{cross}} \tag{21}$$

Here A_{cross} is the cross-sectional area of the pipe, being equal to πR^2 (in which R is the pipe radius).

When waves appear at the liquid-liquid interface, the wave amplitude can be defined as

$$A = \sqrt{2\overline{(\delta - \bar{\delta})^2}} \tag{22}$$

Here δ is the instantaneous thickness of the annulus; an overbar denotes the averaged value (in space and time). The amplitude is defined

such that it gives the usual value of the amplitude for the case that the wave is a pure sinus (where the amplitude is half the difference between the maximum and the minimum value

2.5. Averaging

The first order and second order statistics of the RANS and DNS results will be determined by averaging in the main streamwise direction (i.e. the pipe direction x) and in time. This is done as follows.

(Total) water holdup fraction

$$\alpha_w = \frac{\iint \alpha \; dxdt}{\iint dxdt} \tag{23}$$

Here α is the local water holdup fraction. Note that the total water holdup fraction α_w is the same quantity as defined in Eq. (19).

(Total) oil holdup fraction

$$\alpha_o = 1 - \alpha_w = \frac{\iint (1-\alpha) \; dxdt}{\iint dxdt} \tag{24}$$

Mixture velocity

$$U_m = \frac{\iint u \; dxdt}{\iint dxdt} \tag{25}$$

Superficial water velocity

$$U_{sw} = \frac{\iint \alpha \; u \; dxdt}{\iint dxdt} \tag{26}$$

Superficial oil velocity

$$U_{so} = \frac{\iint (1-\alpha) \; u \; dxdt}{\iint dxdt} \tag{27}$$

Turbulent kinetic energy

$$k^+ = \frac{1}{\rho_w u_\tau^2}\left[\left\langle \rho \frac{1}{2}(u^2+v^2+w^2)\right\rangle - \langle\rho\rangle \frac{1}{2}\left(\langle u\rangle^2 + \langle v\rangle^2 + \langle w\rangle^2\right)\right] \tag{28}$$

Here the brackets $\langle\rangle$ refer to averaging according to:

$$\langle\chi\rangle = \frac{\iint \chi \; dxdt}{\iint dxdt} \tag{29}$$

The wall shear velocity u_τ appearing in the plus scaling of the turbulent kinetic energy follows from:

$$\rho_w u_\tau^2 = \tau_w = -\frac{R}{2}\frac{dp}{dx} \tag{30}$$

Here $-dp/dx$ is the imposed pressure gradient, and τ_w is the corresponding wall shear stress.

Reynolds shear stress

$$\overline{u_i u_j}^+ = \frac{1}{\rho_w u_\tau^2}\left[\langle \rho u_i u_j\rangle - \langle\rho\rangle\langle u_i\rangle\langle u_j\rangle)\right] \tag{31}$$

The expressions above apply averaging with respect to the streamwise coordinate x and the time t. For simulations without gravity these average quantities will be axi-symmetric, i.e. only dependent on the radial coordinate r. Therefore for results obtained without gravity, the averaging is also done in azimuthal direction (in addition to averaging over x and t), as this will gives a faster convergence of the statistics.

When a turbulence model is used, like the Launder & Sharma low-Reynolds-number $k-\varepsilon$ model within RANS in the presented study, part of the contribution to the turbulent kinetic energy and to the Reynolds stress is already covered by the closure relations used in the model. However, there is also a part due to the waves moving at the interface. In the presentation of the average RANS results the modeled part and the wave part will be added to give a single value for the (total) turbulent kinetic energy and the (total) Reynolds stress.

The dynamic simulations were started with a certain initial field, and the simulation was carried out over a sufficiently long time until a stationary state was established. Thereafter, the average values were determined over an averaging time of typically 1 s. To verify the statistics, the obtained values were compared with those obtained at double the averaging time. To get an estimate of the required averaging time, the typical turbulent eddy turn-over time can be estimated as the ratio of the order of the eddy mixing length (say $0.1*D$=0.1*0.021=0.0021 m) and the eddy velocity (say 0.1 U_{mix}= 0.1*1.24=0.124 m/s). This gives an eddy turn-over time of 0.0021/0.124=0.017 s. An averaging time of 1 s thus contains about 60 eddy time unit, which is indeed a typical averaging time applied in DNS.

3. RANS and DNS for single phase pipe flow

Both RANS simulations and DNS were carried out for single-phase water flow through a pipe.

3.1. DNS at $Re_D \approx 5300$

To validate the performance of OpenFOAM for direct numerical simulation of turbulent flows, first single-phase water pipe flow was tested. The same flow conditions as used by Eggels et al. (1994) are considered. In their case, Re_τ=180 was simulated, in which the shear-based Reynolds number is defined as $Re_\tau = u_\tau R/\nu$ (here the wall shear velocity can be expressed as $u_\tau = \sqrt{\tau_w/\rho}$, where τ_w is the wall shear stress). Eggels et al. used a staggered grid in a pipe section with a length equal to 5 times the pipe diameter. In our simulation, we are using a collocated grid with a pipe section length of 6 times the pipe diameter. $Re_\tau = 180$ corresponds to a Re_Dvalue of about 5300. Here $Re_D = U_m D/\nu$ (in which U_m is the mean velocity, D is the pipe diameter, and ν is the kinematic fluid viscosity).

To resolve the small-scale turbulent structures in pipe flow, the mesh size needs to be sufficiently small enough. The smallest scale is the Kolmogorov length scale: $\eta = D{\cdot}Re_D^{-3/4}$. For DNS, it is important to solve the turbulent dissipation, in which the energy of the macro structures is cascaded to micro structures. According to Pope (2000), the peak value of the dissipation spectrum is not at η but at 10 η, and most of the energy is dissipated at 3 η. For turbulent pipe flow, resolving the Kolomogorov length scale means having a grid size of order one in plus units (a plus value denotes non-dimensionalization with ν and u_τ). According to Moin and Mahesh (1998), the required mesh size is also dependent on the numerical method. We have carried out simulations at successively refined meshes and found almost mesh-independent results when using Δr^+=1.3, $R\Delta\Theta^+$=3.5, and Δx^+=4.5, as shown in Table 1. For the verification of the simulation accuracy, we consider the Fanning friction factor, which is the non-dimensionalized pressure gradient according to:

$$f = -\frac{dp}{dx}\frac{R}{\rho u_m^2} \tag{32}$$

Table 1
Fanning friction factor obtained with DNS with different mesh resolutions for single phase pipe flow at $\boldsymbol{Re_\tau} = 180$.

Method	Mesh (x,r,θ)	Δx^+	Δr^+	$R\Delta\theta^+$	Fanning friction factor
DNS – present	240 × 60 × 160	9	2.6	7	0.0091
DNS – present	480 × 120 × 320	4.5	1.3	3.5	0.0092
DNS – Eggels et al. (1994)	256 × 96 × 128	7	1.9	9	0.0092
DNS – Wu & Moin (2008)	512 × 256 × 512	5.3	0.7	2.2	0.0094
DNS – Pirozzoli et al. (2021)	256 × 67 × 256	10.5	2.7	4.4	0.0093

Table 1 shows that the Fanning friction factor as obtained with the present DNS on the finest mesh is close to the DNS predictions by Eggels et al. (1994), Wu and Moin (2008), and Pirozzoli et al. (2021). The value of Δr^+ in the table is the average mesh size in radial direction; in the actual simulation a non-equidistant mesh is used which refines the mesh when the wall is approached, such that there are grid cells that are small enough to be located within the viscous sublayer along the pipe wall. See section 2.2. for a description of the mesh that was used in our own simulations.

A snapshot of the instantaneous streamwise velocity is shown in Fig. 1. The outer cylindrical plane is close to the wall, and has a dimensionless distance $(R-r)^+$ of about 7. Low speed streaks can be seen in this plane. In the cross section, according to Eggels et al. (1994), the velocity field is similar to a jet flow hitting the wall, which is due to the "impingent effect": high-speed fluid from the centre hits the wall, and energy is transfered to the azimuthal and streamwise directions.

Fig. 2 compares the present DNS results with literature values for the average streamwise velocity (non-dimensionalized with u_τ), the turbulent kinetic energy, and the Reynolds stress. There is very good agreement between the current and existing DNS predictions.

The comparison demonstrates that OpenFOAM code is able to perform rather accurate DNS once a sufficiently fine mesh is used.

3.2. Comparison between DNS/ RANS for single phase pipe flow

RANS with the Launder & Sharma low-Reynolds number $k-\varepsilon$ model was used to simulate single phase pipe flow at Re_τ=180 and 1140, corresponding to Re_D of about 5300 and 44000, respectively. The RANS results were obtained by solving the 1D axi-symmetric equations on a very fine grid (giving mesh independent results).

The profiles for the average streamwise, the turbulent kinetic energy, and the Reynolds shear stress are compared in Fig. 3. The DNS results for Re_τ=180 were obtained in the present study, but the DNS at Re_τ=1140 are due to Pirozzoli et al. (2021). All the RANS results were obtained in the present study. Compared to the DNS, RANS significantly underpredicts the turbulent kinetic energy in the boundary layer along the pipe wall, whereas the Reynolds shear stress is in good agreement. At the higher Reynolds number Re_τ=1140, the RANS prediction of the averaged streamwise velocity, non-dimensionalized with the wall shear stress u_τ, is close to the DNS profile. For the lower Reynolds number of Re_τ=180, the RANS velocity profile is somewhat above the DNS profile. This is consistent with the lower value of the Fanning friction factor with RANS compared to DNS, as is shown in Fig. 4. The friction factor with DNS (taken from the literature, Wu & Moin 2008 and Pirozzoli et al. 2021) is very close to the experiments (by Toonder & Nieuwstadt 1997, and Zagarola & Smits 1998), in a range of Reynolds numbers up to Re_D of one million. RANS (with Launder & Sharma low-Re $k-\varepsilon$) gives an underprediction of the Fanning friction factor in the lower Reynolds number range. For example, the RANS value for the Fanning friction factor is 0.0078 at Re_D =5300 versus 0.0092 with DNS (i.e. 15% lower), and 0.0050 at Re_D =44000 versus 0.0053 with DNS (i.e. 6% lower).

This RANS/DNS comparison for single phase turbulent pipe flow is relevant for understanding core-annular flow with a turbulent annulus, as will be shown in the subsequent sections of this paper.

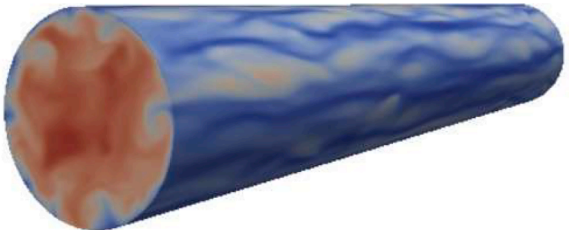

Fig. 1. DNS result for instantaneous streamwise velocity in single phase pipe flow at $\boldsymbol{Re_\tau}$ = 180. (lower values in blue, and higher values in red).

4. RANS and DNS for annulus flow with fixed wavy interface

In core-annular flow, interfacial waves appear due to the apparent slip effect between the oil and water. As shown in detail by Li et al. (2023b) for the turbulent water annulus, the instability is inertia driven (i.e. Kelvin-Helmholtz type). The interfacial waves are important for the levitation of the viscous core in a horizontal pipe; note that the term levitation refers to the phenomenon that the core is eccentric in upward direction, though without touching the upper pipe wall. To study the interaction of the interface waves and the turbulent annulus, single phase simulations are carried out for the water annulus. This is done by assuming that the oil core moves as a solid body in which the interface appears as a travelling solid wavy wall. The assumption is based on the fact that the oil is around 1000 times more viscous than water.

To perform the single-phase simulation that represents a two-phase problem, a pressure drop term is added to the right-hand side of Eq. 2. The pressure drop is calculated at each iteration step in the numerical solver, by balancing the wall shear stress with the pressure drop acting on the whole pipe volume section, i.e. the combination of the simulated turbulent water annulus and the solid oil core. This numerical method has been verified for the RANS model by Li et al. (2021). In this section, the same procedure has been used for DNS in the annulus. The average values obtained with the DNS are compared with the RANS results. Note that gravity effects are ignored which gives concentric average profiles. This approach has the great benefit that only single-phase DNS have to be performed, which is much cheaper than multiphase DNS while it still gives insight in the behaviour of two-phase flow.

4.1. Geometry and mesh

The geometry for the annulus flow is shown in Fig. 5; considered is a pipe section in a reference frame that is moving with the oil velocity that is set to 1.3 m/s. This means that the pipe wall in the reference frame is moving with a velocity of -1.3 m/s. The water hold-up fraction of the annulus (i.e. the ratio of the annulus area and the pipe cross sectional area) is set to 0.257. A wavy sinusoidal-shaped core is imposed as the inner wall of the annulus. The wave length and wave amplitude are taken from our previous 2D two-phase RANS simulation results (Li et al., 2022), namely a wave length of 12.8 mm and a wave amplitude A=0.71 mm. The total flow rate is 0.00043 m^3/s, with a 20% watercut. With the pipe radius being the same as our experimental pipe, namely 10.5 mm, this gives a corresponding mixture velocity of 1.24 m/s. With the holdup fraction of 0.257 and the watercut of 20%, the corresponding holdup ratio h is equal to 1.39. A uniform mesh is applied in the radial, streamwise, and azimuthal directions. Note that because of the curvature of the interface, the radial mesh size is varying along the wave.

To validate the numerical accuracy, several mesh resolutions are simulated. The results for DNS and RANS on the different meshes are summarized in Table 2. Gravity is not included, which means that it suffices to carry out 2D axisymmetric simulations with RANS. Of course, 3D simulations are required for DNS. Upon mesh refinement, both DNS and RANS give almost mesh independent results, in which the Fanning friction factor with RANS is about 15% lower than with DNS.

The mixture-based Reynolds number, $Re_D = U_{mix}D/\nu_w$, for the considered condition is 39000. Single-phase pipe flow at this Reynolds number has a Fanning friction factor of 0.0055 (with an accuracy of 2 decimals) according to the DNS and experiments shown in Fig. 4. The RANS value of 0.0052 (with an accuracy of 2 decimals) for single-phase pipe flow at Re_D = 39000 is slightly lower than the DNS/experimental value of 0.0055. As shown in Table 2, the RANS value of 0.0050 (with an accuracy of 2 decimals) for the annulus flow at Re_D = 39000 (and 20% watercut) is lower than the DNS value of 0.0062 (with an accuracy of 2 decimals).

It is noted that there is no reason why DNS and RANS should

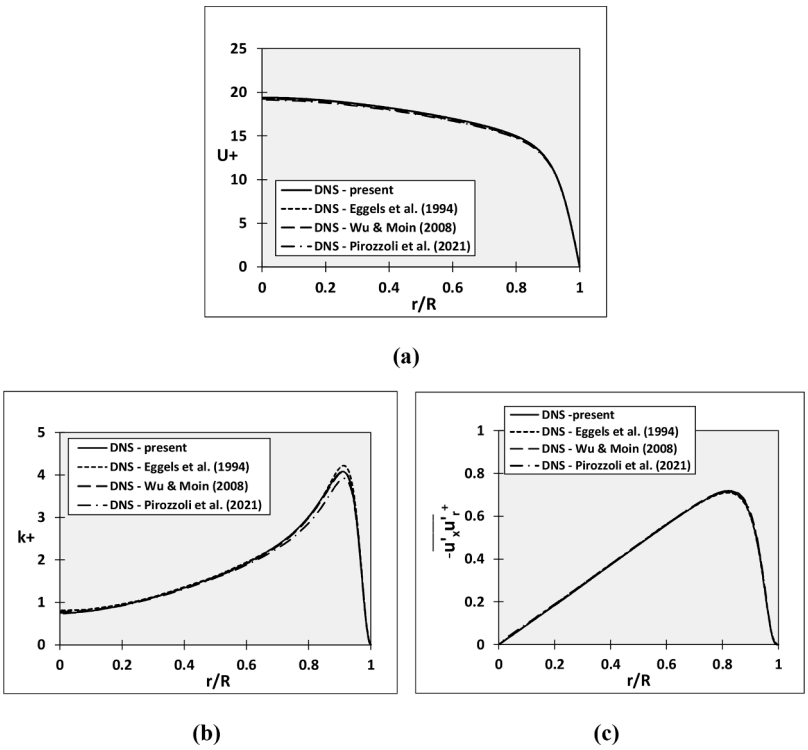

Fig. 2. DNS for single-phase pipe flow at $Re_\tau = 180$; (a) average streamwise velocity, (b) turbulent kinetic energy, (c) Reynolds shear stress.

converge to the same value for the Fanning friction factor upon mesh refinement. In fact, based on the (almost fully mesh-independent) single phase pipe flow results for DNS and RANS in Fig. 4, where the RANS value is lower than the DNS value, also for the annulus flow we expect the mesh-independent RANS prediction for the Fanning friction factor to be lower than the DNS prediction. This is confirmed by the mesh convergence behaviour for the annulus flow in Table 2.

4.2. Averaged flow

Within the moving frame of reference, the 3D unsteady DNS results are averaged in time and in the azimuthal spatial directions to obtain the profiles at the x-coordinates along the wave. The averaged streamwise velocity, turbulent kinetic energy, and Reynolds shear stress are shown in Fig. 6, both at the x locations where the annulus thickness is minimum and maximum. In addition, also the profiles after streamwise averaging are shown. As expected, the turbulent kinetic energy and Reynolds stress are largest in the thickest part of the water annulus. A good indication of the turbulence level is provided by the local value of the shear-based Reynolds number $Re_\tau = d^+ = u_\tau d_w/\nu_w$, in which d_w is the local water annulus thickness; $Re_\tau = 66$ at the location where the water annulus is thinnest and 212 at the location where the water annulus is thickest. The higher the value of Re_τ, the more turbulent the wall layer will be.

Fig. 6 also includes the streamwise averaged DNS profiles, using the definitions given in section 2.5. The profiles in the annulus close to the pipe wall are in very good agreement with DNS for the single-phase pipe flow as obtained by Pirozzoli et al. (2021) for a slightly higher Reynolds number ($Re_D = 44000$ instead of 39000).

The steady state RANS results in the annulus, with respect to the moving frame of reference results, are compared with the average DNS results in Fig. 7 for the streamlines and in Fig. 8 for the turbulent kinetic energy. The recirculation zone along the wavy interface is slightly larger in RANS than in DNS, whereas the turbulence level is slightly smaller in RANS than in DNS.

The differences between RANS and DNS can also be examined through considering the streamwise averaged profiles (using the definitions that were given in section 2.5). Shown in Fig. 9 are (DNS as solid line, RANS as dashed line): the superficial velocities, the turbulent kinetic energy, and the Reynolds shear stress. As the wave pattern along the interface is fixed in these simulations, there is a zero wave-induced contribution to the turbulent kinetic energy and to the Reynolds shear stress. RANS and DNS for the superficial velocities almost coincide. The turbulent kinetic energy in RANS is slightly smaller than in the DNS, whereas the Reynolds shear stress is slightly larger. The shape of the profile for the turbulent kinetic (Fig. 9b) in DNS shows a rather pronounced peak layer close to the wall whereas RANS gives a much broader plateau. This is also noticeable in the turbulence profiles in Fig. 8. A similar difference between DNS and RANS for the turbulent kinetic energy is found for single phase pipe flow, as was shown for $Re_D \approx 5300$ and $Re_D \approx 44000$ in Fig. 3b.

4.3. Wavy interface versus flat interface

To show the effect of interfacial waves on the turbulent annulus flow, the results from DNS and RANS for annulus flow with a flat interface are used for comparison. The annulus flow without wavy interface corresponds to an idealized flow pattern, the so-called perfect core-annular flow (PCAF). This flow pattern is only possible for vertical CAF and will be unstable for horizontal CAF. To obtain the same watercut of 20% as in the simulation with a wavy interface, the water holdup fraction was set to 0.32. Furthermore to keep a mixture velocity of $U_{mix} = 1.24$ m/s (or a total flow rate of 0.00043 m^3/s), the interface velocity (or the oil core velocity) was set to 1.46 m/s. Due to the absence of waves at the interface the Fanning friction factor is significantly reduced from 0.0062 to 0.0033 in DNS and from 0.0052 to 0.0029 in RANS.

The average profiles are compared in Fig. 10. Shown are: the streamwise velocity, the turbulent kinetic energy, and the Reynolds stress. The results are all non-dimensionalized with the mixture velocity U_{mix} (instead of the wall shear velocity u_τ) to reveal how the absence of waves strongly mitigates the turbulence level. At the same mixture velocity of 1.24 m/s and watercut of 20%, the generation of waves at the interface increases the stress between the water annulus and oil core.

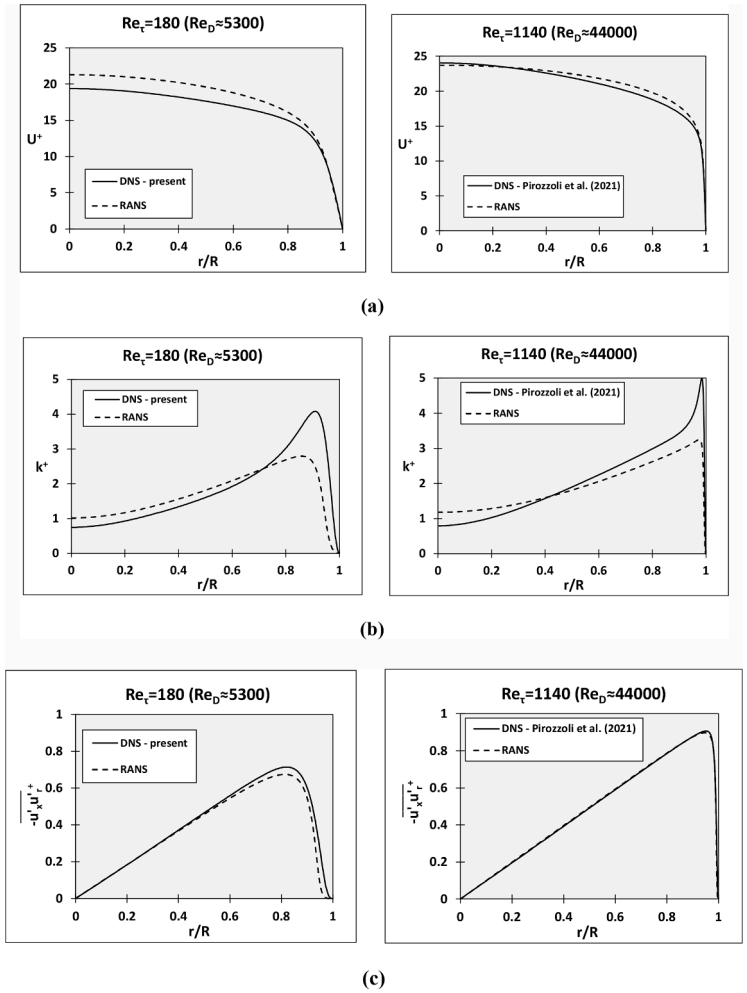

Fig. 3. Comparison between DNS and RANS for single phase pipe flow at Re_D≈5300 (left graphs) and Re_D≈44000 (right graphs); (a) average streamwise velocity, (b) turbulent kinetic energy, (c) Reynolds shear stress.

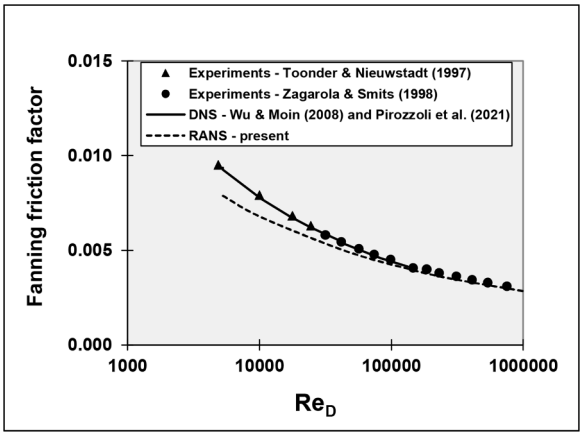

Fig. 4. Comparison of the Fanning friction factor for single-phase pipe flow.

This deceases the thickness of the annulus (i.e. it decreases the water holdup fraction), which in turn increases the average annulus velocity (Fig. 10a). The increased velocity and shear in the annulus, in the presence of waves, is responsible for the strong increase in turbulence as reflected by the higher values of the turbulent kinetic energy (Fig. 10b) and the Reynolds stress (Fig. 10c). The higher annulus velocity also leads to the higher pressure drop (or higher Fanning friction factor) for the wavy interface case. The average shear-based Reynolds number Re_τ remains about the same at 138. Fig. 10 also includes the comparison with single-phase pipe flow. The velocity and turbulence profiles in the annulus in the presence of waves are close to the pipe flow results.

Fig. 11 shows the instantaneous streamwise velocity fluctuation at a distance close to the pipe wall and close to the interface (in fact the distance was taken equal to 7 plus units), for the DNS simulation with wavy interface. Similar to what is known from turbulent pipe flow, also in the annulus longitudinal streaks are found in the turbulent boundary layer close to the pipe wall (Fig. 11a). Along the wavy interface (Fig. 11b), the streaks are also present in the part where the annulus is thin (i.e. along the wave crest seen from the oil core). However, the streaks are broken along the part where the annulus is thick (i.e. along the wave trough). This is the part where the average flow has separated from the interface and gives a recirculation zone with respect to an observer travelling with the wave velocity, as was shown in Fig. 7.

5. RANS and DNS for two-phase core-annular flow without gravity

3D DNS and 2D axisymmetric RANS simulations are performed for two-phase core-annular flow. The conditions are the same as in the annulus simulation from the previous section: 12.8 mm pipe section length, 21 mm pipe diameter, 1.24 m/s mixture velocity, 0.257 total water holdup fraction. Gravity was not included yet. The ratio of the length of the water annulus and the averaged thickness of the annulus is

Fig. 5. Geometry for the annulus flow with a fixed wavy inner wall.

Table 2
Mesh dependence for single-phase annulus simulations at Re_D=39000 and 20% watercut.

	Mesh (x,r,θ)	Fanning friction factor
DNS	150 × 100 × 450	0.0057
DNS	225 × 150 × 675	0.0062
DNS	300 × 200 × 900	0.0062
RANS	50 × 100	0.0059
RANS	100 × 200	0.0054
RANS	200 × 400	0.0051
RANS	400 × 800	0.0050

about 9, which is expected to be sufficient for the turbulent structures to develop. The mesh resolution in the DNS is 150 × 300 × 450 in streamwise, radial, and azimuthal direction, respectively. A structured mesh is used in the whole domain. In the pipe centre, the mesh is built in a pentagon shape to avoid a singular mesh. Since only laminar oil goes through this region, the mesh size and shape are of less importance here. In total, 21 million structured grid cells are used in this DNS. With the high-performance computer resources available for the study, this was the maximum resolution that could be used in the two-phase DNS.

For both RANS and DNS, the resulting values for the Fanning friction factor, the holdup ratio h, and the wave amplitude A are given in Table 3. RANS and DNS values for the holdup ratio and wave amplitude are close. The RANS value of 0.0051 for the Fanning friction factor is very close to the value of 0.0052 found in the single-phase annulus flow simulation. The DNS value of 0.0053 value for the Fanning friction factor is smaller than the value of 0.0062 found for the single-phase annulus flow. We were unable to verify the mesh resolution for the two-phase DNS, as further mesh refinement would require excessively long computer times. Looking at the mesh convergence behaviour for the single-phase DNS in the annulus (see Table 2), it is expected that further mesh refinement for the two-phase DNS would give a slight increase of the Fanning friction factor from 0.0053 (bringing it closer to the single-phase value of 0.0062); but this is somewhat speculative.

The averaged DNS and RANS profiles for the two-phase core-annular flow without gravity are compared in Fig. 12; the solid lines denote DNS and the dashed line RANS results. There is a slight deviation between the two approaches for the superficial velocity. As also found for the single-phase annulus simulations and for the single-phase pipe flow simulations, the RANS prediction for the turbulent kinetic energy is smaller than the DNS prediction. Note that the turbulent kinetic energy and Reynolds stress in RANS now also include a contribution induced by the fluctuating interface wave motion. The Reynolds stress profile in RANS is close to the DNS prediction. The DNS profiles close to the wall in the water annulus are in good agreement with the DNS simulations for the turbulent single-phase pipe flow by Pirozzoli et al. (2021).

The DNS results for the single-phase annulus with imposed wavy interface and for the two-phase core annular flow without gravity are compared in Fig. 13. Shown are: the water holdup fraction, the superficial velocity, the turbulent kinetic energy, and the Reynolds shear stress. The agreement between the two approaches is very good. Only the turbulent kinetic energy in the two-phase DNS is higher than in the single-phase DNS. This is because the two-phase DNS also has a (small) contribution in the kinetic energy and Reynolds stress due to the wave movement (which in contrast to the single-phase simplification no longer has a fixed shape moving with a fixed velocity). Note that the cusp that is visible in the superficial velocity (Fig. 13b) is not a numerical artefact, but it is due to the jump in the first derivative of radial water holdup fraction (Fig. 13a), implied by the imposed sinusoidal wave shape.

The lab experiments for the horizontal core annular flow show a rather concentric flow (i.e. only a small eccentricity due to the density difference between the oil and water). Therefore, it makes sense to compare the oscillations of the thickness of the water annulus at a certain streamwise location, as simulated with the DNS and RANS approach without gravity (i.e. on-average concentric flow), with the experiments; see Fig. 14 for the comparison with the experiments in the top and bottom water annulus. The simulated frequency in both DNS and RANS is close to the experimental value. Also the wave amplitude in the simulations (0.78 mm for DNS and 0.73 mm for RANS) is close to the measured value (0.78 mm in the top layer and 1.13 mm in the bottom layer).

6. RANS, DNS, and experiments for two-phase horizontal core-annular flow with gravity

3D RANS simulations and 3D DNS for two-phase core annular flow were carried out for the same conditions as in the previous sections, but now with inclusion of gravity for the horizontal pipe. The section used in RANS is twice the DNS length (25.6 mm versus 12.8 mm). Due to the difference in density between the oil and the water (902 versus 993 kg/m^3) there will be buoyancy to bring the oil core into an eccentric position in the direction of the upper pipe wall. A compensating pressure force will develop along the wavy oil-water interface such that the net upward force at the interface is equal to the downward gravity force of the oil core. In core annular flow an equilibrium will be found at an eccentric location where the top of the oil core still does not wet the upper pipe wall.

The mesh applied in the DNS is the same as used for the two-phase case without gravity, as presented in the previous section, i.e. 150 × 300 × 450 points in streamwise, radial, and azimuthal direction. For the RANS, 100 × 200 × 160 points are used. The resulting values for the Fanning friction factor, holdup ratio h, and the eccentricity e are summarized in Table 4. The eccentricity is defined as:

$$e = \frac{d_{bottom} - d_{top}}{d_{bottom} + d_{top}} \tag{32a}$$

Here d is the averaged thickness of the water annulus. The DNS and RANS results are also compared with experiments obtained for the same conditions in the oil-water flow loop in our lab. The observations are as follows:

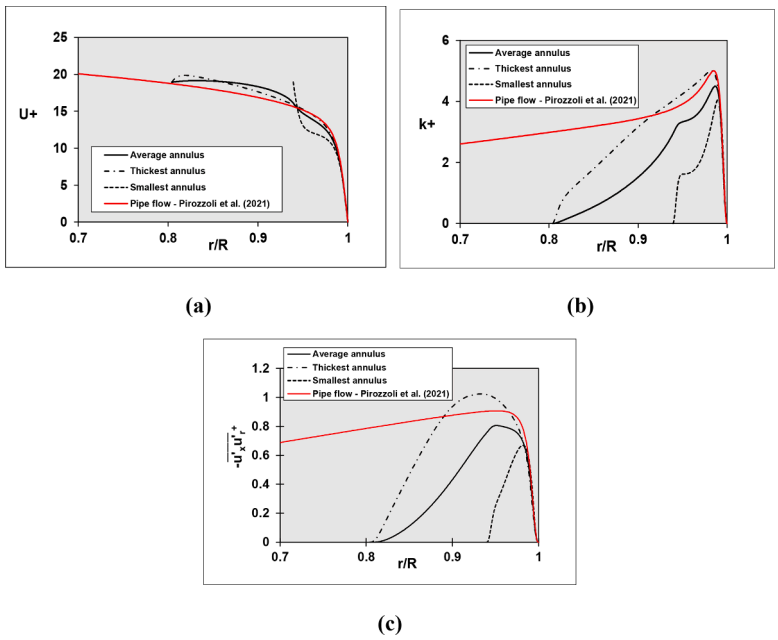

Fig. 6. Single-phase DNS for annulus flow; (a) streamwise velocity, (b) turbulent kinetic energy, (c) Reynolds stress.

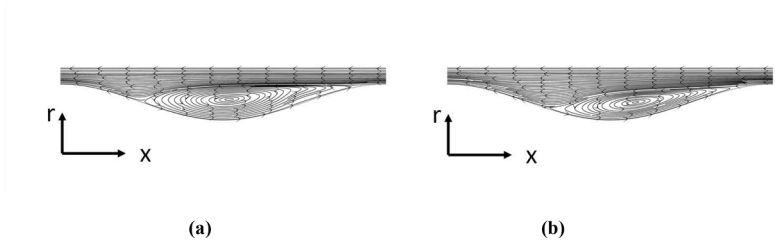

Fig. 7. Streamlines in averaged results with respect to moving wavy interface in simulations for the annulus; (a) RANS, (b) DNS.

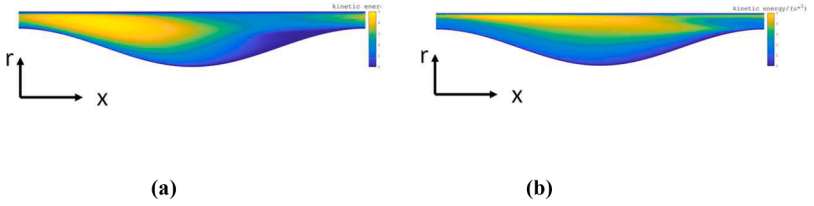

Fig. 8. Turbulent kinetic energy k^+ with respect to moving wavy interface in simulations for the annulus; (a) RANS, (b) DNS. (lower values in blue, and higher values in yellow).

- The Fanning friction factor and holdup fraction in the DNS with gravity are very close to the DNS results without gravity (compare Tables 3 and 4; 0.0052 versus 0.0053). However, DNS with gravity has some eccentricity.
- RANS with gravity has a significantly lower Fanning friction factor than RANS without gravity (0.0042 versus 0.0051)
- The experimental Fanning friction factor is significantly above the DNS and RANS predictions. The experimental flow is much more concentric than the DNS and RANS predictions, though DNS is more concentric (and thus closer to the experiment) than RANS.

The superficial velocities in the top annulus, bottom, and side annulus as obtained with RANS and DNS are compared in Fig. 15. Results are close in the top and side layer, but the deviation is larger in the bottom layer. As shown in Fig. 16, the same is true for the turbulent kinetic energy in the top and side layer, but a larger deviation is found in the bottom layer. In fact there is a large suppression of the kinetic energy and Reynolds stress for RANS in the bottom layer. The difference seems to be due to the occurrence of oil droplet dispersion in the bottom water annulus, as found for RANS, whereas no dispersion occurs in the DNS. The oil-in-water dispersion in the bottom layer is shown in Fig. 17. Even though the dispersed oil droplets take a very small amount of volume, the highly viscous droplets cause a suppression of the turbulence and even a locally relaminarized flow. This also explains the reduction in the Fanning friction factor for RANS in the two-phase flow with gravity (as compared to DNS for the same configuration, and as compared to RANS in two-phase flow without gravity, in which no droplets were found). It is emphasized that the oil droplets found in the RANS simulations for the case with gravity are a numerical artifact, as the mesh is too coarse to represent the physics of their formation and dispersion. However, once artificially present in the simulation, they suppress turbulence and give a (too) low pressure drop (or friction factor).

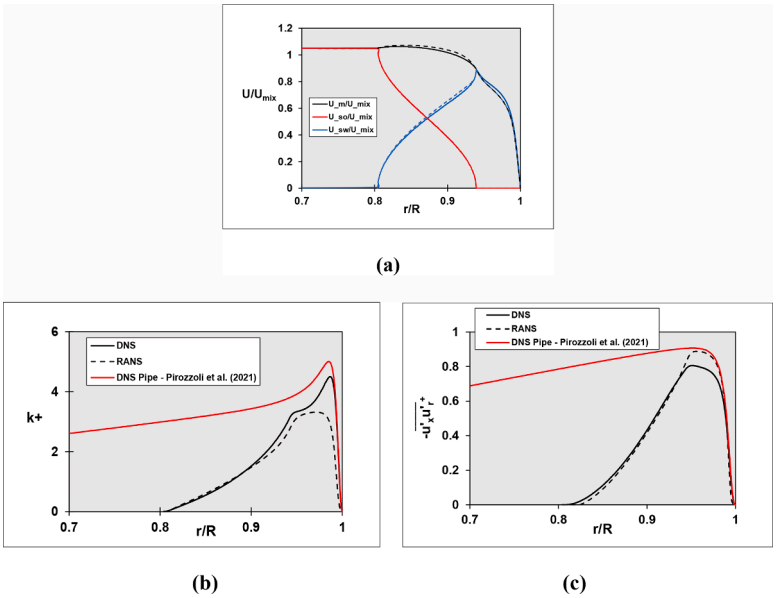

Fig. 9. Comparison of DNS and RANS for single-phase annulus flow (DNS as solid line, RANS as dashed line); (a) streamwise superficial velocity, (b) turbulent kinetic energy, (c) Reynolds shear stress.

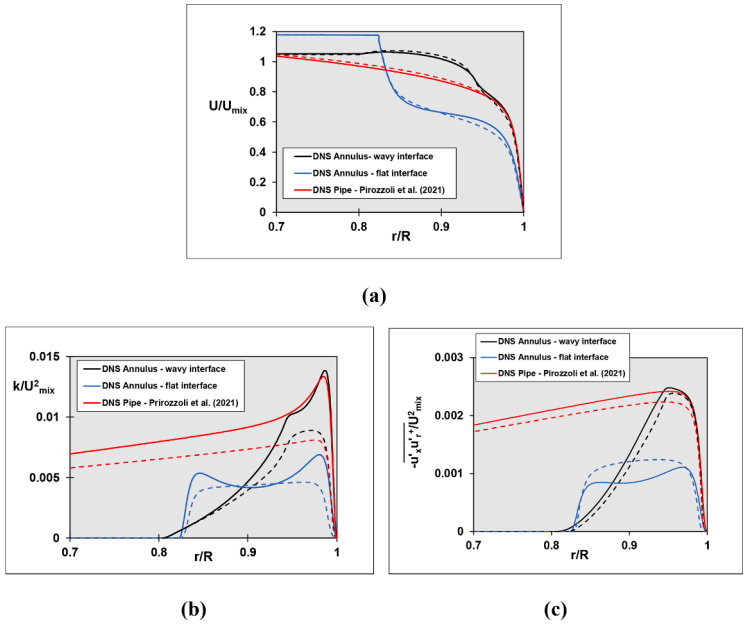

Fig. 10. Single-phase annulus flow with and without waves at the interface (DNS as solid line, RANS as dashed line); (a) streamwise superficial velocity, (b) turbulent kinetic energy, (c) Reynolds shear stress.

Details on the core eccentricity are given in Fig. 18. Here Fig. 18a shows the average location of the oil-water interface in the cross-sectional plane (averaging is done in streamwise direction and over time). Fig. 18b–d, show the average water holdup fraction in the cross-sectional plane along a vertical line to the top, vertical line to the bottom, and along a horizontal line to the side, respectively. The RANS and DNS results are relatively close to each other, but there is a significant deviation with the experimental values. Albeit that the DNS values are somewhat closer to the experiments than the RANS values. The deviation between the DNS and experiments is unexpected, as DNS does not contain any closure correlations. There can be a shortcoming in the obtained DNS, in the obtained experiments (or in both). The applied numerical grid may still be insufficient and the experiment may have suffered from insufficient flow control (like a remaining effect of the bend in the pipe upstream of the pipe section). There may also be an effect of the still relatively low turbulence level in the water annulus, giving transitional flow rather than fully developed flow. The higher Fanning friction factor in the experiments than in the simulations can be due to a higher turbulence level in the experiment, which can in turn have an effect on the core position. The tendency of laminarization in the simulations may enhance the difference in flow in the top and bottom annuli, leading to an increase in eccentricity.

Finally, Fig. 19 compares the time evolution of the thickness of the water annulus at the top and bottom (at a fixed streamwise location), comparing the simulations (RANS and DNS) with the experiments. In fact the agreement for the fluctuating annulus thickness between the simulations and experiments is less good for the simulations with gravity (i.e. with eccentricity, shown in Fig. 19) than for the simulations without

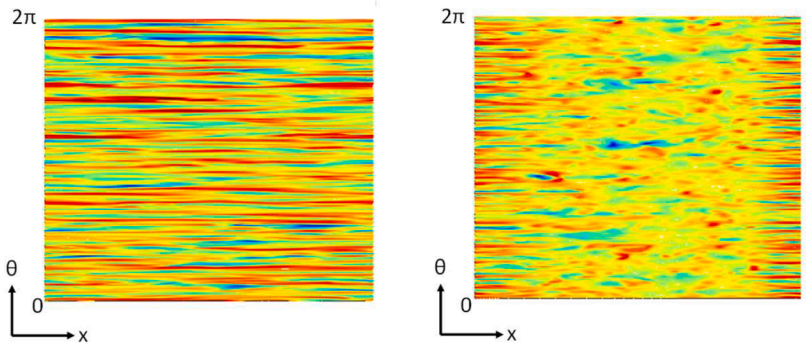

(a) (b)

Fig. 11. Snapshot of instantaneous streamwise velocity fluctuation in the DNS of the water annulus with wavy interface; (a) at small distance (7 plus units) from pipe wall, (b) at small distance (7 plus units) from interface. (positive values in red, and negative values in yellow).

Table 3
Two-phase core-annular flow without gravity.

	Mesh (x,r,θ)	Fanning friction factor	h	Wave amplitude A (mm)
DNS	150 × 300 × 450	0.0053	1.27	0.78
RANS	100 × 200	0.0055	1.24	0.71
RANS	200 × 400	0.0051	1.22	0.73

gravity (i.e. concentric, shown in Fig. 14).

7. Conclusions

DNS and RANS simulations were carried out for core-annular flow in a horizontal pipe and results were compared with experiments carried out with water and oil in our lab. The main conclusions are the following:

- There is very good agreement between the present DNS for single-phase straight pipe flow with benchmark values available in the literature. Compared to DNS and experiments, RANS (with Launder & Sharma low-Re $k-\varepsilon$) gives an underprediction of the Fanning friction factor by 6% at Re_D=44000. Compared to the DNS, RANS significantly underpredicts the turbulent kinetic energy in the boundary layer along the pipe wall, whereas the Reynolds shear stress is in good agreement.
- Simulating the *single-phase* water annulus with an imposed moving wavy interface is an attractive method to get insight into core-annular flow, without the need to carry out *two-phase* simulations. In this way very accurate 2D RANS and 3D DNS results could be obtained. The considered mixture-based Reynolds is Re_D = 39000. The DNS value of 0.0055 for water-only pipe flow at this Reynolds number is only slightly higher than the RANS value of 0.0050 for the annulus and slightly lower than the DNS value of 0.0062 for the annulus. The recirculation zone along the wavy interface is slightly larger in RANS than in DNS, whereas the turbulence level is slightly smaller in RANS than in DNS. As the wave pattern along the interface in these simulations has a fixed shape and moves with a constant

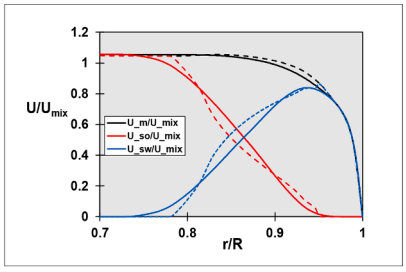

(a)

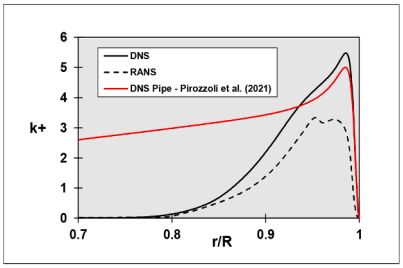

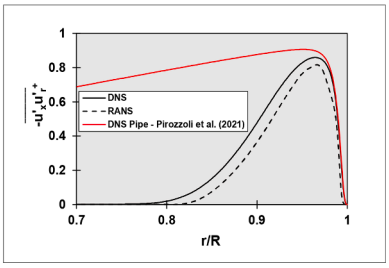

(b) (c)

Fig. 12. Comparison of DNS and RANS for two-phase core-annular flow without gravity; (a) streamwise superficial velocity, (b) turbulent kinetic energy, (c) Reynolds shear stress.

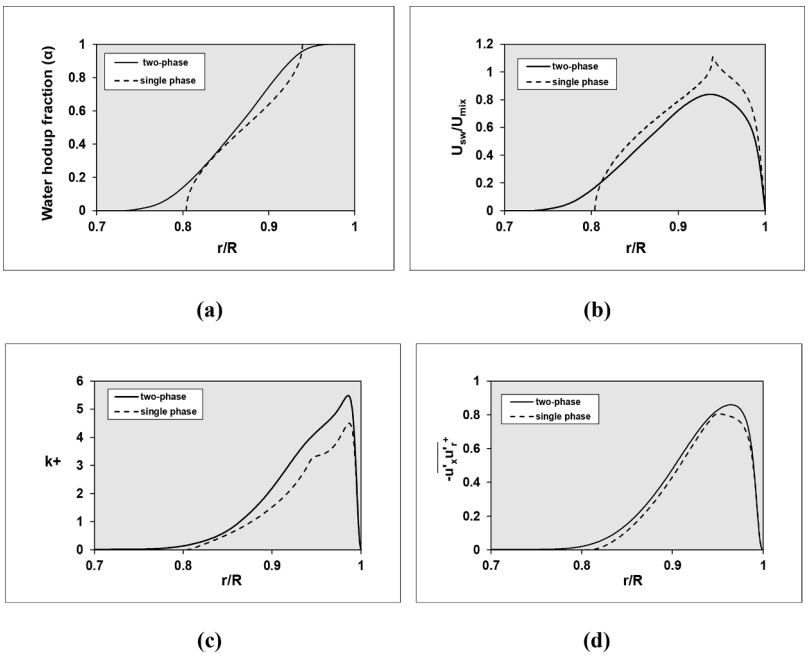

Fig. 13. Comparison of single phase and two-phase DNS (without gravity); (a) water hold-up fraction, (b) streamwise superficial water velocity, (c) turbulent kinetic energy, (d) Reynolds shear stress.

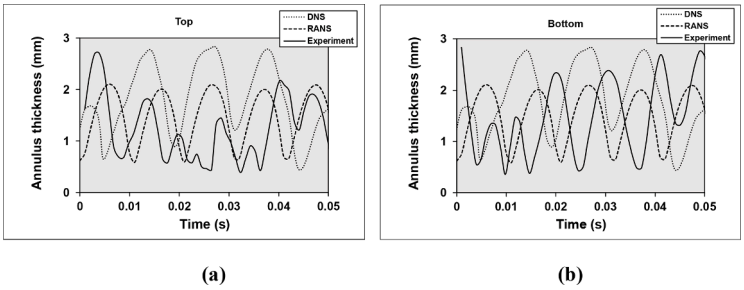

Fig. 14. comparison of time dependent thickness of the water annulus for DNS (without gravity), RANS (without gravity), and experiments; (a) top layer, (b) bottom layer.

Table 4
Fanning friction factor for two-phase core-annular flow with gravity.

	Mesh (x,r,θ)	Fanning friction factor	h	Eccentricity
Experiment		0.0077	1.41	0.12
DNS	150 × 300 × 450	0.0052	1.29	0.47
RANS	100 × 200 × 160	0.0042	1.38	0.73

velocity, there is a zero wave-induced contribution to the turbulent kinetic energy and to the Reynolds shear stress. RANS and DNS for the superficial velocities almost coincide. The turbulent kinetic energy in RANS is slightly smaller than in the DNS, whereas the Reynolds shear stress is slightly larger.

- As demonstrated by the DNS and RANS for the annulus flow, comparing the cases with a flat interface and with a wavy interface (for the same mixture velocity and watercut) reveals that the waves give an increased stress between the core and annulus. This decreases the annulus thickness and increases the velocity in the annulus, which in turn increases the turbulence and increases the pressure drop. The flow in the annulus becomes quite similar to pipe flow, with turbulent streaks along the pipe wall. The streaks are broken along the wave trough at the interface.
- 3D DNS and 2D axisymmetric RANS simulations were performed for *two-phase* core-annular flow without gravity (i.e. with a concentric oil core). The DNS value of 0.0053 for the Fanning friction factor is smaller than the value of 0.0062 found with DNS for the single-phase annulus flow. Whereas mesh refinement for the single-phase DNS showed that the Fanning friction factor is accurate in 2 decimals, mesh refinement for the two-phase DNS was not feasible, as this would require excessively long computer times. It is speculated that mesh refinement for the two-phase DNS would give Fanning friction factor a bit higher than 0.0053, i.e. closer to 0.0062. As also found for the single-phase annulus simulations and for the single-phase pipe flow simulations, the RANS prediction for the turbulent kinetic energy is smaller than the DNS prediction. The Reynolds stress profile in RANS is close to the DNS prediction. There is close agreement between the averaged velocity and turbulence profiles obtained in the two-phase (core-annulus) and the single-phase (annulus) approaches.
- 3D DNS and 3D RANS simulations were performed for *two-phase* core-annular flow in a horizontal pipe with gravity (i.e. with an eccentric oil core). The Fanning friction factor for the DNS with and without gravity are very close (0.0052 versus 0.0053, albeit not fully mesh independent), but RANS with gravity gives a significantly lower value than found without gravity (0.0042 versus 0.0051). The difference seems to be due to the occurrence of oil droplet dispersion

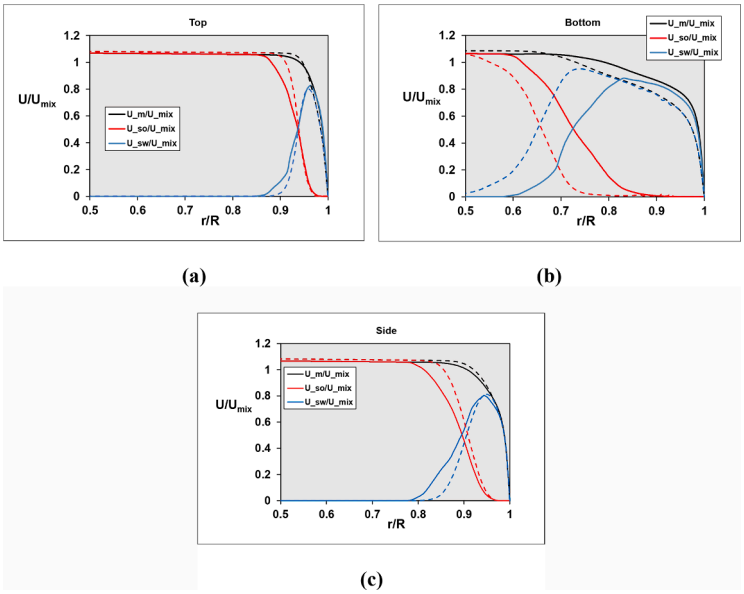

Fig. 15. Streamwise superficial velocity for two-phase horizontal core-annular flow with gravity (DNS/ solid line and RANS/dashed line); (a) top, (b) bottom, (c) side.

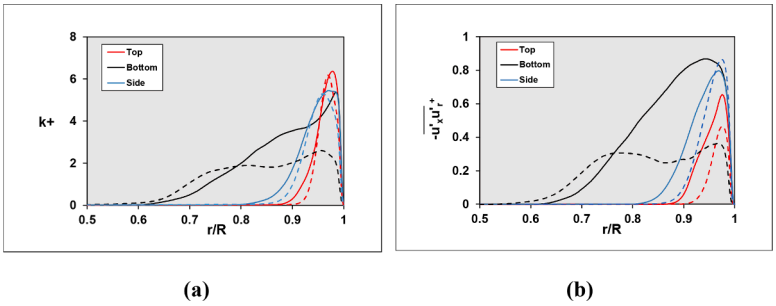

Fig. 16. (a) Turbulent kinetic energy, and (b) Reynolds shear stress for two-phase horizontal core-annular flow with gravity; DNS = solid line and RANS = dashed line.

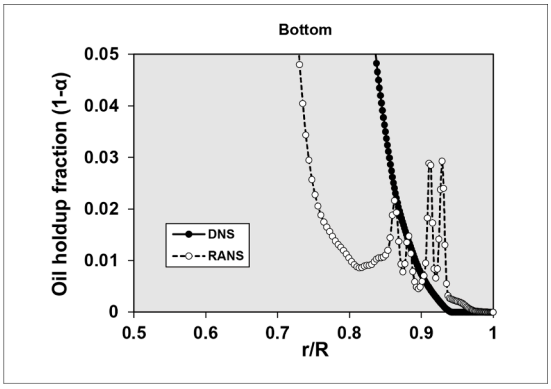

Fig. 17. Oil holdup fraction in bottom layer for two-phase horizontal core-annular flow with gravity; DNS versus RANS.

in the bottom water annulus, as found for RANS, whereas no dispersion occurs in the DNS. The droplets are a numerical artifact, as the mesh is too coarse to properly capture them. The highly viscous droplets cause a suppression of the turbulence and even local relaminarization.

- The experimental Fanning friction factor is significantly above the DNS and RANS predictions (0.0077 in the experiments versus 0.0052 in the DNS). The experimental flow is much more concentric than the DNS and RANS predictions, though DNS is more concentric (and thus closer to the experiment) than RANS. The cause for the differences between simulations and experiments is not clear yet. It might be due to the still relatively low turbulence level in the water annulus, giving transitional flow rather than fully developed flow. The higher Fanning friction factor in the experiments than in the simulations can be due to a higher turbulence level in the experiment, which in turn can have an effect on the core position.

In this paper, we have built up complexity in the considered cases: single-phase pipe flow (DNS/RANS) → single phase annulus flow (DNS/RANS) → two-phase flow without gravity (DNS/RANS) → two-phase flow with gravity (DNS/RANS). In the latter, seemingly quite complex case, we are faced with the limitations on what can be done. This can serve as the basis for further research on core-annular flow. There is a need for more accurate and faster numerics for such two-phase flows (e.g. to prevent spurious droplet formation in the RANS and to obtain the friction factor with two decimals accuracy) but also additional experiments with an advanced experimental technique to measure gravity effects and eccentricity.

CRediT authorship contribution statement

Haoyu Li: Conceptualization, Formal analysis, Methodology,

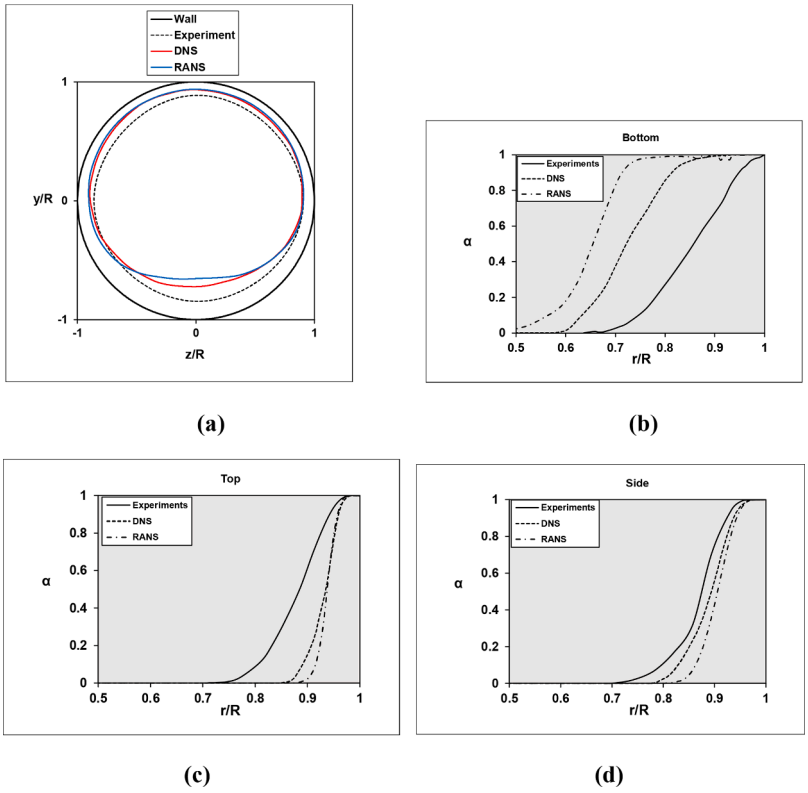

Fig. 18. Interface location and water holdup fraction (α) for two-phase horizontal core-annular flow with gravity; (a) interface location, (b) water holdup fraction in bottom layer, (c) water holdup fraction in top layer, (d) water holdup fraction in side layer.

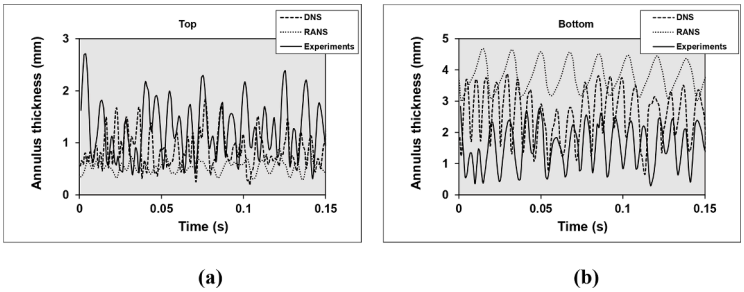

Fig. 19. Time-dependent annulus thickness for two-phase horizontal core-annular flow with gravity; (a) top layer, (b) bottom layer.

Writing – original draft. **M.J.B.M. Pourquié:** Conceptualization, Methodology, Supervision, Writing – review & editing. **G. Ooms:** Conceptualization, Methodology, Supervision, Writing – review & editing. **R.A.W.M. Henkes:** Conceptualization, Methodology, Supervision, Writing – review & editing.

Declaration of competing interest

The authors declare that they have no known competing financial interests or personal relationships that could have appeared to influence the work reported in this paper.

Data availability

Data will be made available on request.

Acknowledgements

The first author has received a grant from the China Scholarship Council (CSC). Thanks are also due the Netherlands Foundation of Scientific Research (NWO) for supplying the computer time.

References

Bai, R., Kelkar, K., Joseph, D.D., 1996. Direct simulation of interfacial waves in a high-viscosity-ratio and axisymmetric core-annular flow. J. Fluid Mech. 327, 1–34.
Beerens, J.C., Ooms, G., Pourquié, M.J.B.M, 2014. A comparison between numerical predictions and theoretical and experimental results for laminar core-annular flow. AIChE J. 60, 3046–3056.
Buckley, M.P., Veron, F., 2016. Structure of the airflow above surface waves. J. Phys. Oceanogr. 46, 1377–1397.
Eggels, J.G.M., Unger, F., Weiss, M.H., Westerweel, J., Adrian, R.J., Friedrich, R., Nieuwstadt, F.T.M., 1994. Fully developed turbulent pipe flow: a comparison between direct numerical simulation and experiment. J. Fluid Mech. 268, 175–210.
Ghosh, S., Das, G, Das, P.K., 2010. Simulation of core annular downflow through CFD – a comprehensive study. Chem. Eng. Process. 49, 1222–1228.
Ghosh, S., Mandal, T.K., Das, P.K., 2009. Review of oil water core annular flow. Renew. Sustain. Energy Rev. 13, 1957–1965.
Giamagas, G., Zonta, F., Roccon, A., Soldati, A., 2023. Turbulence and interface waves in stratified oil-water channel flow at large viscosity ratio. Flow, Turbulence, and Combustion 1–17.
Huang, A., Christodoulou, C., Joseph, D.D., 1994. Friction factor and hold up studies for lubricated pipelining part. 2: Laminar and k–epsilon models of eccentric core flow. Int. J. Multiphase Flow 20, 481–491.

Ingen Housz, E.M.R.M., Ooms, G., Henkes, R.A.W.M., Pourquie, M.J.B.M., Kidess, A., Radhakrishnan, R., 2017. A comparison between numerical predictions and experimental results for core-annular flow with a turbulent annulus. Int. J. Multiphase Flow 95, 271–282.
Jiménez, J., Moin, P., 1991. The minimal flow unit in near-wall turbulence. J. Fluid Mech. 225, 213–240.
Joseph, D.D., Bai, R., Chen, K.P., Renardy, Y.Y., 1997. Core-Annular Flows. Ann. Rev. Fluid Mech. 29, 65–90.
Kang, M., Shim, H., Osher, S., 2007. Level set-based simulations of two-phase oil–water flows in pipes. J. Sci. Comput. 31, 153–184.
Kim, K., Choi, H., 2018. Direct numerical simulation of a turbulent core-annular flow with water-lubricated high viscosity oil in a vertical pipe. J. Fluid Mech. 849, 419–447.
Ko, T., Choi, H.G., Bai, R., 2002. Finite element method simulation of turbulent wavy core–annular flows using a k–ω turbulence model method. Int. J. Multiphase Flow 28, 1205–1222.
Launder, B.E., Sharma, B.T., 1974. Application of the energy dissipation model of turbulence to the calculation of flow near a spinning disc. Lett. Heat Mass Transf. 1, 131–138.
Li, H., Pourquié, M.J.B.M., Ooms, G., Henkes, R.A.W.M., 2021. Simulation of turbulent horizontal oil-water core-annular flow with a low-Reynolds number k-ϵ model. Int. J. Multiphase Flow 142, 103744.
Li, H., Pourquié, M.J.B.M., Ooms, G., Henkes, R.A.W.M., 2022. Simulation of turbulent annulus with interfacial waves in core-annular pipe flow. Int. J. Multiphase Flow 154, 104152.
Li, H., Pourquié, M.J.B.M., Ooms, G., Henkes, R.A.W.M., 2023a. Simulation of vertical core-annular flow with a turbulent annulus. Int. J. Multiphase Flow 167, 104551.
Li, H., Pourquié, M.J.B.M., Ooms, G., Henkes, R.A.W.M. 2023b. Interfacial wave growth for core-annular pipe flow with a turbulent annulus. Submitted for publication.
Li, J., Renardy, Y., 1999. Direct simulation of unsteady axisymmetric core–annular flow with high viscosity ratio. J. Fluid Mech. 391, 123–149.
Moin, P., Mahesh, K., 1998. Direct numerical simulation: a tool in turbulence research. Ann. Rev. Fluid Mech. 30, 539–578.
Ooms, G., Pourquié, M., Beerens, J.C., 2013. On the levitation force in horizontal core-annular flow with a large viscosity ratio and small density ratio. Physics of Fluids 25, 032102.
Pirozzoli, S., Romero, J., Fatica, M, Verzicco, R., Orlandi, P., 2021. One-point statistics for turbulent pipe flow up to Reτ≈6000. J. Fluid Mech. 926, 355–377.
Pope, S.B., 2000. Turbulent Flows. Cambridge University Press.
Shi, J., Gourma, M., Yeung, H., 2017. CFD simulation of horizontal oil-water flow with matched density and medium viscosity ratio in different flow regimes. J. Pet. Sci. Eng. 151, 373–383.
Sullivan, P.P, McWilliams, J.C., Moeng, C.H., 2000. Simulation of turbulent flow over idealized water waves. J. Fluid Mech. 404, 47–85.
Toonder, J.M.J., Nieuwstadt, F.T.M., 1997. Reynolds number effects in a turbulent pipe flow for low to moderate Re. Physics of Fluids 9, 3398–3409.
Wu, X., Moin, K., 2008. A direct numerical simulation study on the mean velocity characteristics in turbulent pipe flow. J. Fluid Mech. 608, 81–112.
Yamamoto, T., Okano, Y., Dost, S., 2017. Validation of the S-CLSVOF method with the density-scaled balanced continuum surface force model in multiphase systems coupled with thermocapillary flows. Int. J. Numer. Methods Fluids 83 (3), 223–244.
Yousefi, K., Veron, F., Buckley, M.P., 2020. Momentum flux measurements in the airflow over wind-generated surface waves. J. Fluid Mech. 895, A15.
Zagarola, M.V., Smits, A.J., 1998. Mean flow scaling in turbulent pipe flow. J. Fluid Mech. 373, 33–79.